Journal of Catalysis 405 (2022) 24–34

Contents lists available at ScienceDirect

Journal of Catalysis

journal homepage: www.elsevier.com/locate/jcat

The many roles of solvent in homogeneous catalysis - The reductive amination showcase

Froze Jameel, Matthias Stein *

Max Planck Institute for Dynamics of Complex Technical Systems, Molecular Simulations and Design Group, Sandtorstrasse 1, 39106 Magdeburg, Germany

ARTICLE INFO

Article history:
Received 6 September 2021
Revised 5 November 2021
Accepted 8 November 2021
Available online 16 November 2021

Keywords:
Sustainable catalysis
Solvent design
Homogeneous catalysis
Reaction mechanism
Reaction kinetics
Transition metal

ABSTRACT

In the global effort to fight climate change, the design and development of novel procedures for complex chemical multi-step reactions is essential for the transformation of chemical industry. The transformation of chemical production processes from petrochemicals towards renewable, sustainable feedstock and the identification of green solvent candidates require a careful assessment of the effects of solvent on thermodynamics and kinetics. As a prime example for the many roles of solvent in chemical catalysis, the reaction mechanism of the homogeneous rhodium-catalyzed reductive amination of 1-undecanal from plant oils with diethylamine forming the long-chain tertiary *N,N*-diethylundecylamine is investigated. The many roles of solvent during the course of a chemical reactions become apparent when direct substrate-solvent and catalyst-solvent interactions are considered and their polarization effects. Hydrogen bond forming solvent molecules promote the enamine intermediate formation in terms of thermodynamics and kinetics by actively participating as proton transfer agents but a de-solvation penalty for polar groups compromises the overall pathway. The sophisticated bidentate phosphine (SulfoXantPhos)RhH reducing catalyst controls the regioselectivity of the reaction by dedicated ligand-substrate interactions. Its activity is critically dependent on the strength of solvent coordination. The effect of solvent on the reaction rate becomes apparent from a solvent screening of the transition state of the rate-determining step and give a perspective on solvent control of rate constants in this complex multi-step reaction. Only in presence of an appropriate solvent, the calculated Gibbs free potential energy surface becomes shallow and flat and delivers thermodynamic and kinetic parameters in good agreement with experiment.

1. Introduction

Technological progress is the key to novel, lasting solutions to economic and environmental challenges. Promoting sustainable industries, key scientific research and innovation are required for such sustainable development. Novel processes in the chemical industry drive the transformation procedure from fast depleting fossil-fuel-based towards sustainable feedstock from oil and fat as raw materials [1]. In 2015, the United Nations' Sustainable Development Goals' [2] call for the urgency of actions on economic, social, and ecological fronts to ensure safe and secure living by 2030.

Amines are widely used key intermediate chemicals with a wide range of applications in agriculture, pharmaceutical, food, and water treatment industries [3]. In particular, aliphatic amines are a versatile feedstock and key intermediate for the production of polymers and therapeutics [4].

One of the most attractive methods to obtain aliphatic amines is the reductive amination of aldehydes [5]. (Scheme 1) Reductive amination initiates with the nucleophilic addition of an amine to the carbonyl group of the aldehyde, forming a hemiaminal, and a subsequent dehydration step results in an enamine or an imine. Recent mechanistic studies have shown that the enamine pathway is favored in neutral media [6]. In contrast, protonation of either the aldehyde or amine nitrogen in the presence of an acid leads to the imine or iminium as intermediates [7]. High pressure *in situ* NMR experiments on the hydroaminomethylation reaction with rhodium diphosphine as catalyst confirmed the presence of the enamine species before hydrogenation [8]. The tertiary amine is obtained via hydrogenation of enamine in the presence of transition metal catalyst and hydrogen gas (Scheme 1).

Hydrogenation of the enamine by molecular hydrogen as a reducing agent is the choice for large-scale amine formation [9].

* Corresponding author.
E-mail address: matthias.stein@mpi-magdeburg.mpg.de (M. Stein).

https://doi.org/10.1016/j.jcat.2021.11.010
0021-9517/

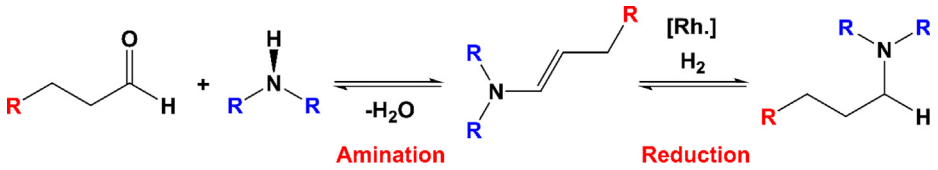

Scheme 1. Production of long-chain diethylamines from aldehydes via reductive amination.

Homogeneous [10-12] and heterogeneous [13-19] catalysts were employed for the reductive amination and enabled milder reaction conditions (from 250 °C and 125 bar [20]) to 100 °C and 30 bar [21]. Various transition metal catalysts using nickel [5], iridium [22-24], cobalt [25], ruthenium [12,26-28], molybdenum, iron, manganese, and tin (reviewed in detail in reference [9]) were used to activate molecular hydrogen and accelerate the hydrogenation step. Rhodium catalysts [10,21,22,29,30] are preferred due to their ability to catalyze both hydroformylation and reductive amination, thus allowing a direct synthesis of tertiary amines from alkenes in a tandem hydroaminomethylation reaction [31].

Catalytic phosphine-containing ligands are efficient in the hydroformylation reaction step and, in particular, bulky bidentate electron-donating ligands, such as XantPhos, are appreciated for their high activity and linear/branched selectivity in the reductive amination [21,30,32]. Their steric hindrance is responsible for a high regio- and chemoselectivity due to reduced isomerization of alkenes, the successive hydride transfer to the coordinated C = C double bond and β-proton abstraction. In a hydroaminomethylation setup, 99:1% linear vs. branched amines are produced from linear alkenes [33]. Since the solubility of XantPhos is low in a polar media, water-soluble sulfonated XantPhos can be synthesized in the presence of sulfuric acid at 5℃ [34]. When Rh(acac)(cod) is used as a precursor and SulfoXantphos as ligand, a highly active hydrogenation catalyst in terms of reaction rate and selectivity is obtained [21,30].

Recent review articles give a comprehensive overview of advanced catalyst-ligand systems for tandem hydroaminomethylation [31] and transition metal-catalyzed reductive amination [9] but do not discuss mechanistic and computational work in detail. Computational approaches have, so far, focused either on mechanistic aspects of the amination step [6,7,35], a simplified model-based description of the hydrogenation event [6], or only the transition-metal catalyzed hydrogenation step [36,8,25,37]. This results in a discussion as to the nature of the overall rate-determining step along the full reductive amination process due to the use of different computational methods, which hinders the direct comparison of results. Here, we show for the first time a full mechanistic picture along the entire reductive amination path from the aldehyde to the amine.

The reductive amination is a prime example reaction for the many roles of solvents in homogeneous catalysis. Explicitly coordinating solvent molecules to the aldehyde lead to a significant decrease in the transition state barrier for the initial nucleophilic attack [6,35]. The presence of an acid as a co-catalyst changes the reaction pathway away from the enamine as an intermediate towards the imine or iminium [6,7].

There is a general consensus that the active catalytic species in the hydroformylation of alkenes and enamine hydrogenation ought to be identical [8]. Either a cationic Rh species [21] or a Rh(I)-hydride were discussed, with the latter just being characterized and assigned by *in-situ* ^{1}H NMR studies [27].

Previous quantum chemical studies revealed some mechanistic insight into the reaction but used simplified models for the catalyst and/or substrate. Thus, they do not consider the steric and electronic control of bulky bidentate ligands with regard to substrate binding and reduction. It is the combination of a sterically demanding bidentate ligand with aromatic phenyl rings and its electron-donating property that explains the high regioselectivity of Rh-hydride catalysts. Also, the effects of solvents on kinetics and thermodynamics were not fully taken into account. Therefore, a comprehensive quantum mechanical mechanistic study considering all elementary steps from aldehyde and a secondary amine to a long-chain tertiary amine is not yet available.

Experimental studies have shown that hydrogen bond donating solvents significantly affect the rate and selectivity of the reductive amination compared to the polar (without hydrogen bonding abilities) and non-polar media [38,39]. The commonly used polar aprotic dimethylformamide (DMF) is a coordinating solvent and obstructs enamine access to the Rh catalyst. Its strong binding to the catalyst and degradation at elevated temperature explains the reduced turnover and product selectivity. Here, we present for the first time a complete and comprehensive mechanism for the reductive amination of 1-undecanal and diethylamine to give *N,N*-diethylundecylamine in a mixed methanol/dodecane solvent system. A particular emphasis is on the effect of solvent on the thermodynamics and transition state barriers of each elementary reaction step. In a cluster-continuum model, different experimental solvent compositions are investigated. An appropriate choice of solvent ought to be favorable for both thermodynamics and kinetics and essential to drive the reaction along a smooth and shallow potential energy surface.

In the transformation process of chemical production, the use of alternative feedstock from renewable sources to replace petrochemicals is needs to be taken into account. Undecanal from plant oil [40] is converted into *N,N*-diethylundecylamine, a lubricating oil. The long and hydrophobic chain poses a particular challenge in terms of solubility and separability; also binding and reduction of the long chain enamine intermediate to the Rh-catalyst (substrate coordination) is more complex due to its rotational flexibility. Long chain substrate-ligand interactions are occurring, which are not present when using short chain petro-chemicals.

Since direct catalyst-solvent (e.g. the explicit coordination of solvent molecules) and ligand-substrate interactions (non-covalent through space interactions between ligand and substrate) play pivotal roles in driving the kinetics and thermodynamics of the reductive amination reaction, explicit consideration of these is necessary when discussing process optimization and green solvent selection. Alternatives will significantly reduce the overall environmental impact and enable the development of more sustainable chemistry processes.

2. Computational details

All DFT calculations were performed using TURBOMOLE V 7.4 2019 [41]. Structures were optimized using the PBE0 [42,43] hybrid functional with D3 dispersion corrections [44] and Becke-Johnson damping [45] using an Ahlrichs'triple-ξ valence polarization [46] (def2-TZVP) basis set for all atoms. This functional was shown to give reliable and consistent reaction energies and thermodynamic corrections for transition-metal catalyzed reactions

(MOR41) [47]. Gibbs free energies were calculated from statistical mechanics within the harmonic approximation by calculating the thermal corrections at experimental operating conditions of 100 °C and 30 bar.

All optimized structures were characterized as minima by calculating 2nd derivatives and absence of any negative frequency. Transition states showed only one imaginary frequency. An initial guess for transition states structures was made through relaxed energy scans along the reaction coordinate. The negative vibrational motion was referring to the formation/breakage of the bond along the reaction coordinate. Dynamic reaction coordinate scans (DRC) [48] were performed along the reaction coordinate in backward and forward directions (number of optimization cycles set to 300) by following the imaginary vibrational mode in both directions to verify the connectivity of the transition state with reactants and products, respectively. DRC becomes equivalent to the intrinsic reaction coordinate scan (IRC) when the damping of velocities is set to zero (setting '–d 0') [49,50].

Solvent effects were calculated using a cluster-continuum model where the solvent molecules in the first solvation shell are explicitly considered at the DFT level. The optimum number of explicit solvent molecules was estimated using the approach suggested by Pliego and Riveros [51]. The implicit COSMO (Conductor like Solvation MOdel) [52] and COSMO-RS (Conductor like Solvation Model for Real Solvents) V.19.0.4 (R 5514) [53] at the BP86/TZVPD-FINE with BP_TZVPD_FINE_19 parameters were used to represent bulk solvent effects. Single point COSMO calculations were performed at the same level of theory (PBE0(D3)/def2-TZVP), at which the structures were optimized using the respective dielectric constant.

Gibbs free energies of solvation were calculated using the standard COSMO-RS procedure [54]. ΔG_{solv} is the change in Gibbs free energy from the pure compound gas phase to the solvated phase, with a reference state of 1 mol/L in both phases. Gibbs free energies of solvation were calculated at infinite dilution using different experimental solvent compositions of methanol:dodecane 50:50 and 99:01 (w/w) solution.

3. Results and discussion

3.1. Reaction mechanism

Thermodynamic and kinetic parameters of the reductive amination in solution were estimated employing quantum chemical methods. The reaction between 1-undecanal and diethylamine leading to the long chain tertiary amine *N,N*-diethylundecylamine in methanol:dodecane 50:50 and 99:01 w/w solutions was investigated (See Fig. 1).

Formation of the enamine from the aldehyde and amine by release of water proceeds in absence of a catalyst; however, the formation of the final product via amination (enamine **5**) requires the Rh-hydride catalyst. We investigated the effect of hydrogen bonding solvents (here methanol) on each step of the chemical reaction in a cluster-continuum approach [51]. When considering explicit coordination of solvent molecules, an estimate of the optimum number of explicit solvent molecules is required. Pliego and Riveros [51] suggested that usually the first solvation shell must be treated explicitly since it corresponds to the largest incremental change in the free energy of solvation. Second and further shells of solvent do not contribute significantly to the free energy of solvation of the solute and an entropic penalty has to be paid upon further cluster solvation. In addition, we were interested in the role of the sterically demanding and bulky diphosphine ligand in determining the catalyst's selectivity as the long chain enamine coordinates to the Rh(SulfoXantPhos) catalyst. There is general consensus regarding the effectiveness of electronic rich diphosphine ligands for hydrogenation reactions as they accelerate the hydride insertion and oxidative addition of hydrogen [55].

The reaction starts with the association of substrates in polar hydrogen bond donating solvent (methanol), forming a pre-complex $\mathbf{2_n}$ (where n = number of explicit solvent molecules coordinated to the catalytic center), followed by the nucleophilic attack of diethylamine to the undecanal and formation of a hemiaminal ($\mathbf{3_3}$) intermediate. Water is released as a result of a two-step intramolecular condensation where at first OH^- is dissociating, forming $\mathbf{4_3}$, followed by proton abstraction from the second carbon to form the enamine ($\mathbf{5_3}$). Consistent with the previously reported NMR and DFT studies, we assume a (SulfoXantPhos)Rh-hydride as active catalyst species (**7**) for the hydrogenation of the enamine. Upon dissociation of a solvent molecule, a free binding site at the catalyst is generated (**6**), where the substrate enamine subsequently binds, thus generating complexes **8** and **8-*rot***. Hydride migratory insertion into the enamine forms the alkylamine complexes (**9** and **9-*rot***). Later, H_2 coordination to the metal center (**10** and **10-*rot***) is followed by an oxidative addition to the catalyst (**11** and **11-*rot***). Finally, the tertiary amine product is released as a result of the reductive elimination reaction.

3.2. Solvent-assisted amination

Diethylamine (DEA) and 1-undecanal (*n*-aldehyde) **1** form the intermediate (E)-*N,N*-diethylundec-1-en-1-amine (enamine) **5** upon release of one water molecule. We have previously reported that enamine formation is almost thermoneutral (ΔG_r = -2 kJ/mol) in solution at 373 K and 30 bar [21]. A simple continuum solvent representation can approximately describe the thermodynamics of amination reaction but is insufficient for estimating solvent effects on kinetics. As the reaction is carried out in a polar and protic solvent (here methanol), the hydrogen bonding effect of the solvent on the thermodynamics of the reaction must be considered.

The carbonyl oxygen of the long-chain *n*-aldehyde has two electron lone pairs hence it act as a hydrogen bond acceptor of two methanol molecules. In the most plausible scenario, diethylamine acts as a hydrogen bond donor and forms a hydrogen bond with one methanol, enhancing the amine's basic character. When the nitrogen lone pair of diethylamine is the hydrogen bond acceptor of a methanol proton, the amine's lone pair is not available for the nucleophilic attack to the carbonyl group. This binding situation is feasible but the barrier for the nucleophilic attack is high (~150 kJ/mol, see Supporting Information).

Since experiments are carried out at an elevated pressure of 30 bar [21], the explicit formation of hydrogen bonds between solvent and solute is very well feasible.

Fig. 2 shows the effect of solvent on the thermodynamics of amine nucleophilic attack on the aldehyde (**A**) and the transition state barrier for the first proton transfer (**B**).

In the absence of solvent, the change in Gibbs free energy upon association of diethylamine and 1-undecanal is 18 kJ/mol, which slightly decreases by 0.6 kJ/mol in pure dodecane but increases by 7 and 8 kJ/mol in methanol:dodecane mixtures of 50:50 and 99:1, respectively.

Methanol may act as a hydrogen bond donor to the carbonyl oxygen and simultaneously as an acceptor of the proton from diethylamine. This reduces the Gibbs free energy of association by 5.8 kJ/mol. When implicit solvent effects are taken into account, it increases again by 1.4, 13.5, and 15.4 kJ/mol in pure dodecane and methanol:dodecane 50:50 and 99:1 mixed solvents, respectively. The origin of this increase in energies of association is the de-solvation penalty that increases with solvent polarity.

A second methanol molecule may form another hydrogen bond to the carbonyl oxygen, but it reduces the Gibbs free energy of

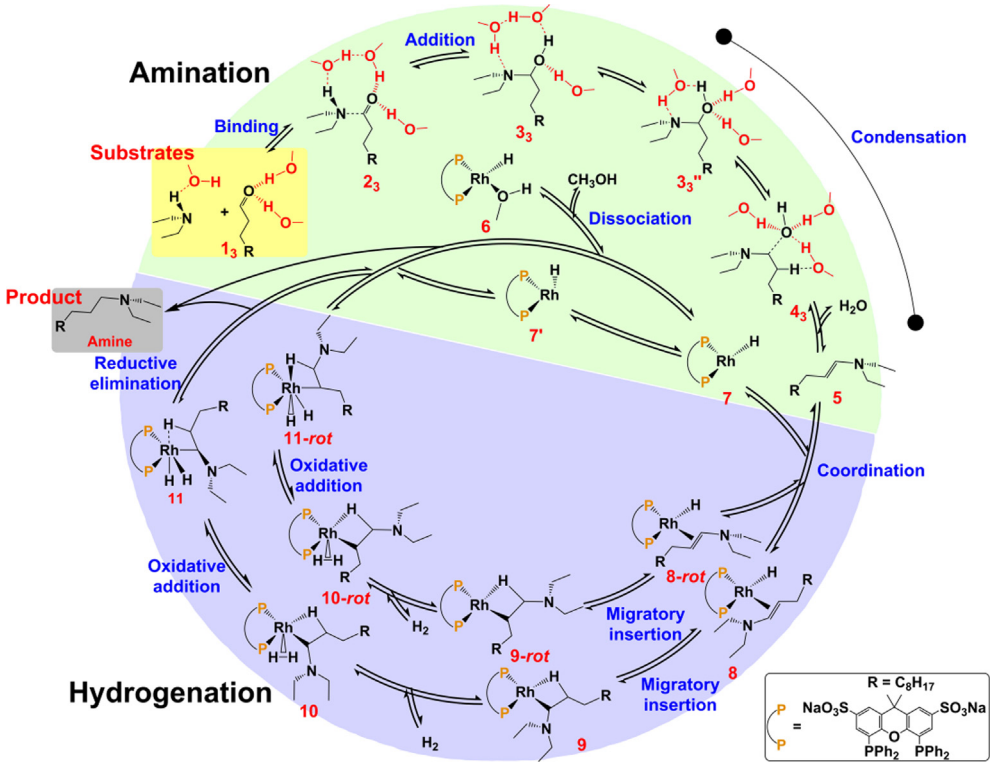

Fig. 1. Synthesis of long-chain amines from aldehydes obtained from oleochemicals and diethylamine by a bidentate phosphine Rh-hydride catalyst. Explicit solvent molecules are shown in red. All steps, intermediates, and transition states connecting them are described in the text. (For interpretation of the references to colour in this figure legend, the reader is referred to the web version of this article.)

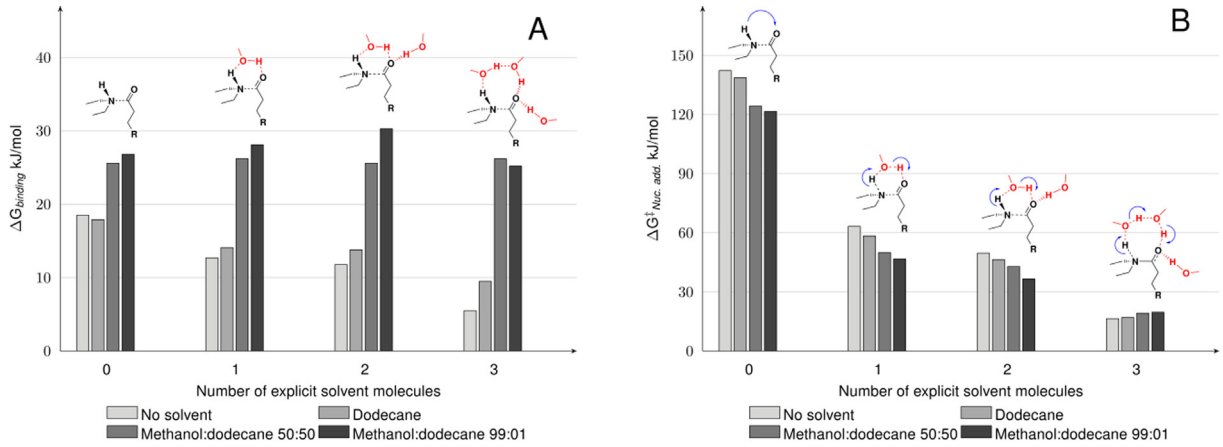

Fig. 2. Solvent effects on the interaction between diethylamine and undecanal in a cluster-continuum model (energies in kJ/mol). **A**: The effect of explicit coordination of methanol molecules on the Gibbs free energy of substrate association. **B**: The effect of explicit solvent interactions on the Gibbs free energy of the transition state for the initial proton transfer from the amine to the aldehyde. Implicit solvation for methanol:dodecane mixtures (w/w 0:100, 50:50, and 99:1).

association by a mere 1 kJ/mol. Implicit solvation slightly destabilizes complex formation and shows the same trend as for the single methanol molecule coordination.

A systematic search for the optimum number of explicit solvent molecules, yielded two methanol molecules that are coordinating to the carbonyl oxygen lone pairs plus one solvent molecule that is bridging between the amine and one solvent (see below and Supporting Information). The addition of a third methanol molecule affords such a cyclic micro-solvation with the lowest Gibbs free energy of association (5.5 kJ/mol). Considering implicit solvation leads to an increase by 4 and 20 kJ/mol in dodecane and mixed methanol:dodecane solutions.

In Fig. 2**B**, the effect of solvent on the transition state (and thus reaction rate) of the initial proton transfer from the amine to the aldehyde is shown. In the absence of any explicit solvation, nucleophilic addition and proton transfer occur simultaneously with an activation energy of 142 kJ/mol. Implicit solvation only has a minor effect on the activation energy barrier and reduces it by 4, 18, and 21 kJ/mol in pure dodecane and methanol:dodecane 50:50 and 99:1.

Explicit coordination of one methanol molecule mediates the proton transfer via a six-membered concerted transition state. Methanol coordination reduces the activation energy barrier by ~80 kJ/mol. With the inclusion of implicit solvation effects, the

barrier is further reduced by 5, 13, and 16 kJ/mol in (0:100, 50:50; 99:1) methanol:dodecane solutions.

Hydrogen bonding of a second methanol molecule to the aldehyde reduces the transition state energy by a further 14 kJ/mol. When implicit solvent effects are included, the Gibbs free energy of activation is only slightly further reduced by 3, 7, and 13 kJ/mol in (0:100, 50:50; 99:1) mixed methanol and dodecane solutions.

When three explicit methanol molecules are considered, the proton from diethylamine is transferred to undecanal via a two methanol proton shuttle. This gives a transition state barrier of 16.4 kJ/mol which is a 126 kJ/mol reduction with respect to the direct proton transfer. The activation energy shows only a minor dependence on the polarity of solvent as in mixed methanol:dodecane solutions (at 0:100, 50:50; 99:1 w/w). It becomes 17, 19, and 20 kJ/mol, respectively.

Following the nucleophilic addition of diethylamine to the undecanal, the subsequent proton transfer leads to the hemiaminal (**3**). Table 1 shows the effects of implicit solvation and explicit methanol coordination on the thermodynamics of hemiaminal formation.

In the absence of any solvent treatment, the Gibbs free energy for hemiaminal formation is −4.9 kJ/mol and is only slightly dependent on the composition of polar/non-polar methanol:dodecane mixed solvents. Non-polar dodecane leads to an increase by 2 kJ/mol in Gibbs free energy, but with increasing methanol composition, the free energy of reaction reaches −4.7 and −5 kJ/mol.

When explicit coordination of one methanol is considered, the formation of the hemiaminal becomes slightly endothermic (2.2 kJ/mol). The consideration of implicit solvent effects lowers the Gibbs free energy by 0.2, 1.5, and 2 kJ/mol in (0:100, 50:50; 99:1) methanol:dodecane solutions and brings it close to a thermoneutral process.

Hydrogen bonding of second explicit methanol significantly affects the thermodynamics of hemiaminal formation. The Gibbs free energy of hemiaminal formation is reduced by 8.8 kJ/mol compared to the single methanol coordinated complex. The Gibbs free energy of the reaction only shows a minor dependence on implicit solvation in mixed methanol:dodecane solutions (at 0:100, 50:50; 99:1 w/w). They become −5.3, −4.4, and −4.5 kJ/mol, respectively.

Three methanol molecules, two of which are coordinating to the carbonyl oxygen lone pairs, and the third is bridging between the amine group and one methanol solvent molecule (see Supporting Information for structural details), constitute the complete first solvation shell. Attempts to incorporate more solvent molecules were unsuccessful and did not improve the energetics any further. The formation of the hemiaminal becomes thermodynamically favored (-12.6 kJ/mol) when three explicit solvent molecules are considered. When implicit solvation is taken into account, it increases by 0.4, 4, and 7.3 kJ/mol in pure dodecane and methanol:dodecane 50:50 and 99:1 mixed solvents, respectively, but is still exothermic and in line with the experimentally determined thermodynamic equilibrium constant of 8.5 M^{-1} corresponding to a Gibbs free energy of −5.4 kJ/mol for hemiaminal formation [56].

3.2.1. Solvent-mediated condensation

Water release from the hemiaminal (**3**) yields (E)-*N*,*N*-diethylundec-1-en-1-amine (enamine) **5.** In an intramolecular condensation reaction, OH^- dissociation and a proton abstraction from the β-carbon occur. Table 2 gives the effects of explicit and implicit solvation on the transition state energies of enamine formation.

In the absence of any solvent, direct water release occurs via a four-membered transition state with an activation energy barrier of 177 kJ/mol (see SI for structural details). Implicit solvation marginally reduces the activation energy by 5, 14, and 17 kJ/mol in pure dodecane and methanol:dodecane 50:50 and 99:1 mixtures.

When one explicit methanol molecule acts as a proton transfer agent, water is released via a six-membered transition state, and the activation energy barrier is reduced by 61 kJ/mol. With the inclusion of implicit solvent effects, the barrier is further reduced by 5, 19, and 22 kJ/mol in (0:100, 50:50, and 99:1) mixed methanol:dodecane solutions.

The Gibbs free energy of the transition state is reduced by further 17 kJ/mol when two methanol molecules assist the condensation step compared to one explicit methanol assistance. It further reduces when incorporating implicit solvent effects by 4, 3, and 6 kJ/mol in pure dodecane, methanol 50:50, and 99:01 mixtures, respectively.

When three methanol molecules are explicitly considered, the formation of the enamine **5** can occur in a concerted or stepwise manner (see Fig. 3). Prior to the water release, a re-orientation of the explicit solvent molecules leads to complexes $\mathbf{3'_3}$ and $\mathbf{3''_3}$, which are both marginally higher in energy relative to the previous intermediate $\mathbf{3_3}$.

In the concerted pathway from $\mathbf{3'_3}$, two solvent molecules form a cyclic structure between the carbonyl oxygen and a proton from the β-carbon. The third molecule forms a second hydrogen bond with the carbonyl oxygen. The re-orientation of solvent molecules from $\mathbf{3_3}$ to $\mathbf{3'_3}$ is almost thermoneutral with a slight change in the Gibbs free energy of + 1.3 kJ/mol, which upon inclusion of implicit solvent effects becomes 2.0, −2.8, and −5.4 (see **Supporting Information** Table S1) in methanol:dodecane mixtures (0:100, 50:50 and 99:1), respectively.

In the concerted mechanism following $\mathbf{3'_3}$, the abstracted proton is transferred to the hydroxide via a two methanol molecule proton shuttle. The activation energy barrier for this pathway is 77 kJ/mol, which is almost 22 kJ/mol lower than for the two methanol case (See Table 2). Implicit solvation only has a minor effect on the activation energy barrier and reduces it by another 1, 2, and 5 kJ/mol in (0:100, 50:50, and 99:01) methanol: dodecane mixtures.

In $\mathbf{3''_3}$, two methanol solvent molecules form hydrogen bonds with the carbonyl oxygen atom, and one methanol forms a cyclic structure acting as a hydrogen bond donor to the hemiaminal nitrogen and as a hydrogen bond acceptor of the hydroxyl group. This re-orientation is associated with a change in Gibbs free energy by 13.8 kJ/mol in the absence of implicit solvation (and lower by 0.4, 2.3, and 4.8 kJ/mol in (0:100, 50:50 and 99:01) methanol:dodecane mixtures).

Following the formation of $\mathbf{3''_3}$, the condensation occurs in a stepwise manner. The solvent-assisted OH^- dissociation leads to a transition state with an increase of the C...OH, distance (from 1.42 to 2.31 Å) and a barrier of 47 kJ/mol due to the stabilization by three strong hydrogen bonds. The activation energy barrier for OH^- dissociation is slightly reduced by 2 kJ/mol in methanol dode-

Table 1
Solvent effects on the formation of the hemiaminal (**3**). Gibbs free energies are given in kJ/mol. The solvent molecules in the first solvent shell were treated explicitly, plus an implicit solvent model for methanol:dodecane mixtures (w/w 0:100, 50:50, and 99:1).

No of explicit solvent molecules	No implicit solvent	Methanol:dodecane (0:100)	Methanol:dodecane (50:50)	Methanol:dodecane (99:01)
0	−4.9	−2.8	−4.7	−5.0
1	+2.2	+2.0	+0.7	+0.2
2	−6.0	−5.3	−4.4	−4.5
3	−12.6	−12.2	−8.6	−4.9

Table 2
Solvent effects on the Gibbs free energies of the transition state of enamine (**5**) formation (in kJ/mol) via a condensation step from the hemiaminal **3**. The solvent molecules in the first solvent shell were treated explicitly while implicit solvent effects were considered for methanol:dodecane mixtures (w/w 0:100, 50:50, and 99:1).

No of explicit solvent molecules	No implicit solvent		Methanol:dodecane (0:100)		Methanol:dodecane (50:50)		Methanol:dodecane (99:01)	
0	177		172		163		160	
1	116		111		97		94	
2	99		95		96		94	
Concerted Release of Water								
3′	77		76		75		72	
Stepwise Release of Water								
3″	47	15	47	18	45	20	45	23

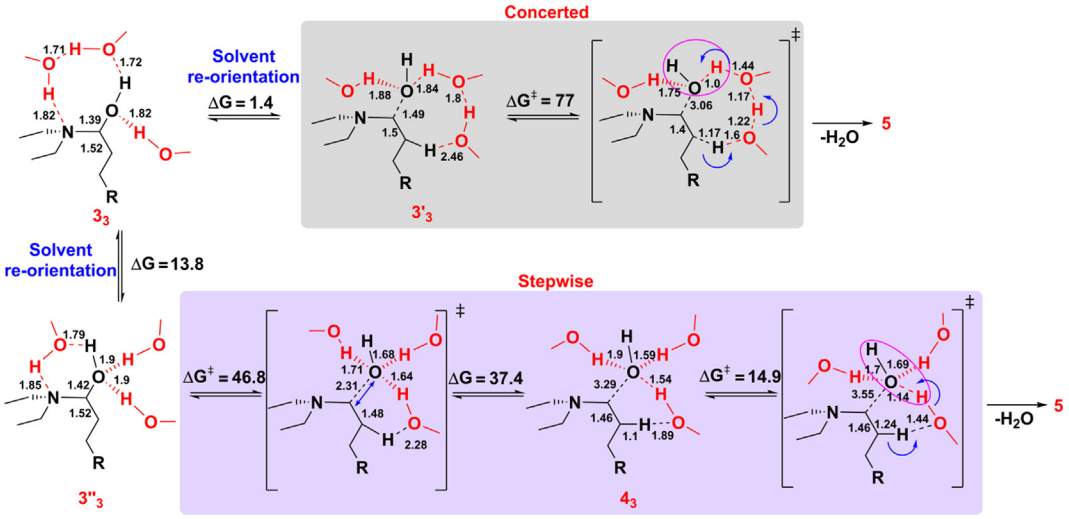

Fig. 3. A concerted and stepwise mechanism for the formation of (E)-*N,N*-diethylundec-1-en-1-amine (enamine) **5** via condensation of carbinolamine intermediates (energies in kJ/mol). Explicit solvent molecules are shown in red, blue arrows depict the proton movement, and the interatomic distances in Å are given in black. (For interpretation of the references to colour in this figure legend, the reader is referred to the web version of this article.)

cane 50:50 and 99:01 mixtures. In the intermediate $\mathbf{4_3}$, the dissociated OH^- is at 3.29 Å from the α-carbon and stabilized by the explicit methanol molecules. One of them is at 1.89 Å to the β-carbon hydrogen atom. The Gibbs free energy of $\mathbf{4_3}$ formation is 37.4 kJ/mol, which reduces by 1.4, 3.4, and 5.2 kJ/mol in pure dodecane, methanol:dodecane 50:50 and 99:01 mixtures. Proton abstraction from the β-carbon in $\mathbf{4_3}$ occurs by one methanol molecule, which is at 1.44 Å distance in the transition state. The activation energy barrier for proton abstraction is 25 kJ/mol in the absence of implicit solvent, which slightly increases by 3, 5, and 8 kJ/mol in implicit solvent. The significant difference in the activation energy barriers suggests that in polar hydrogen bonding solvent, the water release occurs in a stepwise rather than in a concerted fashion.

Fig. 4 shows amination of 1-undecanal and diethylamine to give (E)-*N,N*-diethylundec-1-en-1-amine (enamine) **5** and the effects of explicit solvent coordination on the Gibbs free energy landscape. The Gibbs free energy required for the substrate association decreases by 12.5 kJ/mol when the explicit solvent molecules are taken into account. The activation energy barrier for the nucleophilic addition decreases by 126 kJ/mol when the proton is added to the carbonyl oxygen via a two methanol proton shuttle rather than a direct transfer. The Gibbs free energy required for hemiaminal formation decreases from −4 to −12.6 kJ/mol when explicit solvent coordination is taken into account. In the presence of explicit solvent molecules, condensation of hemiaminal occurs via the kinetically favored stepwise pathway by decreasing the activation energy barrier by more than 120 kJ/mol.

From Fig. 4, it can be seen that explicit solvent molecules alter the shape of the free energy landscape of the amination reaction. Explicit micro-solvation also changes the reaction path from an energetically unfavorable direct to a solvent-assisted low energy stepwise pathway. Explicit solvent assistance flattens the overall potential energy landscape, thus effectively driving the thermodynamics and kinetics of the enamine formation.

3.3. Catalytic hydrogenation of enamine in solution

3.3.1. Catalyst-solvent interactions

Catalytic hydrogenation of the enamine (**5**) by a [Rh]H catalyst leads to the *N,N*-diethylundecylamine product. By catalyst-solvent interaction we refer to the explicit inter-molecular interactions of solvent molecules with the catalyst in solution. The active catalytic species (**7**) (SulfoXantPhos)RhH has a vacant coordination site that is solvent-accessible. Dissociation of a solvent molecule from the pre-catalyst (**6**) is required to generate the reactive square-planar species (**7**) (see Fig. 5). This solvent-catalyst interaction must be energetically balanced. DMF, or its thermal degradation products DMA and CO, bind to the Rh(I) hydrogenation catalyst too strongly, thus obstruct amine reduction [38].

The Gibbs free energy of methanol dissociation is ∼15 kJ/mol in the absence of implicit solvent. It becomes 13 kJ/mol in dodecane and almost thermoneutral with 3 and 2 kJ/mol in methanol:dodecane 50:50 and 99:01 w/w solutions, respectively. At reaction conditions, solvent de-coordination is facile, and active catalyst

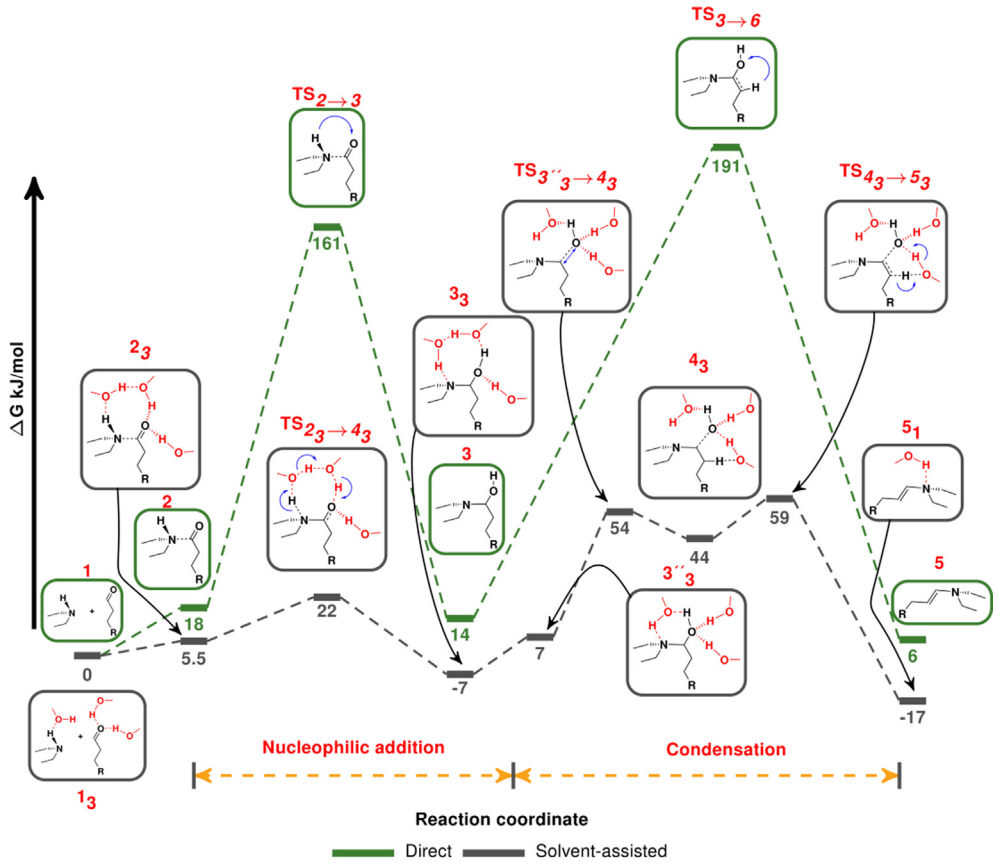

Fig. 4. Gibbs free energy profile of the enamine (**5**) formation from undecanal and diethylamine. All energies are given in kJ/mol. Explicit coordination of methanol molecules significantly affects the reaction mechanism and the potential energy surface (see text for details).

species and solvent-catalyst complex are in equilibrium. This demonstrates the consideration and inclusion of direct solvent-catalyst interactions in reaction media when estimating the concentration of the active catalyst in solution.

The binding energy of the substrate enamine to the active catalyst ($\Delta E_{enamine\ binding}$ = -138 kJ/mol) is significantly stronger than the solvent methanol association with the catalyst ($\Delta E_{methanol\ binding}$ = -81 kJ/mol). Thus, the substrate is able to displace the solvent molecule, coordinate to the Rh-catalyst, and form a tight catalyst-substrate complex **8** (See Fig. 1).

3.3.2. Ligand-substrate interactions

The double bond of the (E)-*N,N*-diethylundec-1-en-1-amine (**5**) binds to the transition metal atom of the catalyst, but the sterically demanding SulfoXantPhos ligand requires a substrate conformational adaptation. Therefore, the long-chain coordinating substrate must re-orient to match the catalyst-ligand pocket.

For the long undecyl and diethylamine chains in **5**, two fundamentally different substrate conformers, **8** and **8-*rot***, are feasible when coordinated with **7** (see Fig. 6). Complex **8** has a square-planar structure with the enamine double bond approximately perpendicular to the (P^P)-RhH plane, and the amine group is facing towards the ligand.

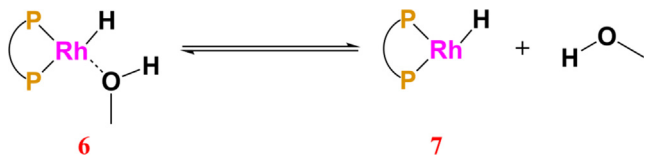

Fig. 5. (SulfoXantPhos)RhH catalyst stabilization via explicit solvent coordination.

In **8-*rot***, the C=C double bond is rotated by almost 180°, and the NEt_2 group is now pointing away from the ligand and facing the solvent. However, the long-chain alkyl rest R is flexible enough to avoid any direct contact with the SulfoXantPhos ligand.

Enamine binding in **8-*rot*** is more favorable by 13 kJ/mol. A direct inter-conversion from **8** to **8-*rot***, however, is not possible due to ligand restrictions; the substrate must dissociate and rebind to form the latter.

Beyond **8** and **8-*rot***, no further catalyst-substrate conformer or rotamer was found due to steric demands of the ligand and the long-chain substrate. The difference in binding modes of **8** and **8-*rot*** can be dissected by different energetic contributions [57]. By $E_{int\text{-}space}$ we refer to the inter-space interaction energy between ligand and substrate (in absence of the transition metal), $E_{int\text{-}bond}$ is the inter-bond interaction energy between the central metal atom and the substrate (in absence of ligand), E_{dist} is the distortion energy of catalyst and substrate from their free conformers.

Inter-bond interactions and distortion energies are the largest energy differences between **8** and **8-*rot*** (see Fig. 7). The higher distortion energy for **8** is partially compensated by the inter-bond interaction energy. For **8-*rot***, the distortion energy is lower, but also catalyst-substrate interaction ($E_{int\text{-}bond}$) is weaker.

Overall, the formation of **8-*rot*** ($\Delta G_{enamine\ binding}$ = -63.2 kJ/mol) is thermodynamically favored compared to **8** ($\Delta G_{enamine\ binding}$ = -49.9 kJ/mol). In mixed methanol:dodecane (0:100, 50:50 and 99:01) solutions, the calculated Gibbs free energies of enamine binding to the catalyst forming complexes **8-*rot*** and **8** are −48, −46.4, −46, and −33, −32, −30 kJ/mol, respectively. Besides the effects on thermodynamics, the effect of ligand-substrate interactions on kinetics is also of interest, which will be discussed below.

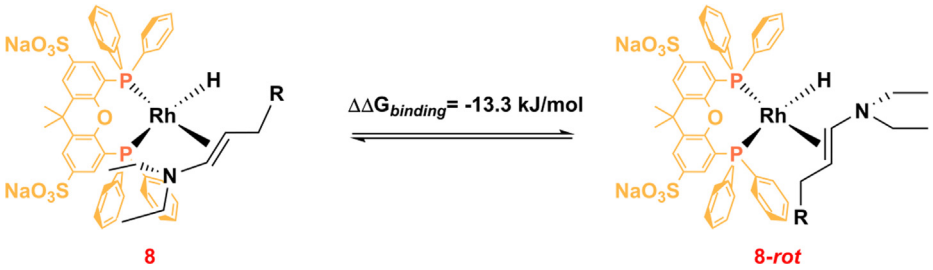

Fig. 6. Enamine binding to a sterically demanding bulky HRh(SulfoXantPhos) catalyst.

3.3.3. Ligand-controlled regioselectivity

Fig. 8 shows the Gibbs free energy profile for the catalytic reduction of conformers **8** and **8-*rot***. Since substrate coordination to **7** completes the rhodium coordination sphere, direct solvent-catalyst interactions are not possible. A rotation of the C=C double bond parallel to the H-Rh bond is necessary for the hydride migratory insertion into the enamine double bond.

Hydride migratory insertion to C_α or C_β leads to the alkylamine complexes **9-*rot*** or **9**, respectively. The sterically demanding SulfoXantPhos ligand hinders C=C bond rotation (see above) which makes the hydride migratory insertion the regioselectivity controlling elementary step for the catalytic reduction of enamine **5**. From 8, the hydride can only bind to C_α, while C_β migratory insertion is impossible due to the restricted C=C bond rotation. In the absence of implicit solvation, the activation energy barrier (**TS 8 → 9**) for hydride binding to C_β is + 23.8 kJ/mol. From 8-**rot**, hydride binding to C_α occurs with a lower activation energy barrier (**TS 8-*rot* → 9-*rot***) of 17.4 kJ/mol without considering solvation. Upon including the solvent effects, the activation energy barriers of both transition states slightly increase by at most 2 kJ/mol.

As a result of hydride binding, square-planar alkylamine complexes **9** and **9-*rot*** are generated containing beta-agostic interactions (see SI for structural details). Formation of **9** and **9-*rot*** is endothermic by 10.01 and 10.07 kJ/mol, respectively. In non-polar dodecane (100:0) and polar methanol:dodecane (50:50 and 99:01) solvent mixtures, the Gibbs free energy for the formation of **9** increases by 3.6, 4.5, and 5.6 kJ/mol. In comparison, the Gibbs free energy for forming **9-*rot*** is almost unaffected with only slight increases of 1.6, 0.7, and 0.7 in methanol:dodecane (0:100, 50:50, and 99:01) solvent mixtures.

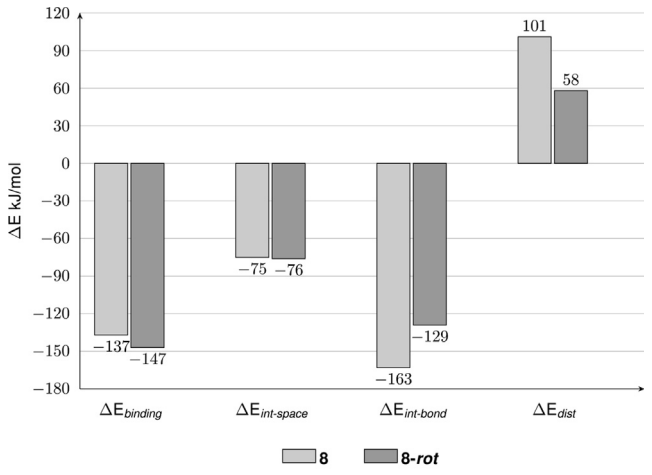

Fig. 7. Analysis of different energy contributions to the (SulfoXantPhos)RhH-enamine interactions in conformers **8** and **8-*rot***.

For the second reduction step, molecular hydrogen binds to the alkylamine complexes **9** and **9-*rot***, thus forming square-pyramidal complexes **10** and **10-*rot***, with H_2 coordinated perpendicular to the (P^P)Rh-alkylamine (See SI for structural details). H_2 coordination is endothermic by 33.8 and 28.3 kJ/mol, and reduced by 4–6 kJ/mol in methanol:dodecane (0:100, 50:50, and 99:01) solvent mixtures.

Oxidative addition of H_2 to the central metal atom (**TS 10 → 11**) occurs without an activation energy barrier. However, **TS 10-*rot* → 11-*rot*** occurs with a small activation energy of +2.5 kJ/mol. There is small energy barrier only in the absence of solvent which disappears when solvation is taken into account. The activation energy of oxidative addition corresponds to the dihydrogen bond splitting and the shift of the agostic interaction from the equatorial to axial plane, thus changing the coordination geometry from square-pyramidal to octahedral.

As a result of H_2 oxidative addition, six-coordinate octahedral (SulfoXantPhos)Rh-HH-(alkylamine) complexes **11** and **11-*rot*** are formed. The Gibbs free energy corresponding to the **11** and **11-*rot*** formation is −19.7 and −14.3 kJ/mol, respectively, which is further decreased by 2.5, 5, and 7 kJ/mol for **11** and by 3.3, 6, and 7 kJ/mol for **11-*rot*** in pure dodecane, methanol:dodecane 50:50, and 99:01 solvent mixtures respectively.

Finally, in the last step, the migratory insertion of the axial hydride to the alkylamine takes place, allowing the formation of the product (*N,N*-diethyldecylamine) along with the catalyst regeneration.

Form each of the two intermediates **11** and **11-*rot***, there are two possibilities for the reductive elimination of the final amine product (See Fig. 8). From complex **11**, the final product's reductive elimination can be achieved via **TS 11 → 7** or **TS 11 → 7′** by overcoming activation energy barriers of 49.2 or 39.5 kJ/mol, respectively. The first case corresponds to the migration of the axial hydride, while the second is the migration of equatorial hydride to the C_α of alkylamine.

When solvent effects are taken into account, the activation energy barrier for **TS 11 → 7** increases by 2.2 kJ/mol in pure dodecane but decreases by 4 and 6 kJ/mol in methanol:dodecane 50:50 and 99:01 solvent mixtures, respectively. In contrast, for **TS 11 → 7′,** the activation energy barrier increase by 5.4, 7.7, and 7.6 kJ/mol in all solvent mixtures.

The difference in activation energy barrier in the absence of solvent between these transition states is almost 10 kJ/mol in favor of **TS 11 → 7′**. The product from (**TS 11 → 7**) is the active catalyst **7** and the desired amine product, however latter (**TS 11 → 7′**) generates a catalytic isomer **7′**, which only upon re-isomerization recovers the active catalyst **7** ($\Delta G_{7'\rightarrow 7}$ = -6.9 kJ/mol). A similar situation applies to the case of complex **11-*rot*,** where either the axial or equatorial hydride approaches C_β of alkylamine. The corresponding activation energy barriers for **TS 11-*rot* → 7** and **TS 11-*rot* → 7′** are 55.8 and 57.2, respectively. The activation energy barrier of **TS 11-*rot* → 7** is almost insensitive to the effects of solvent

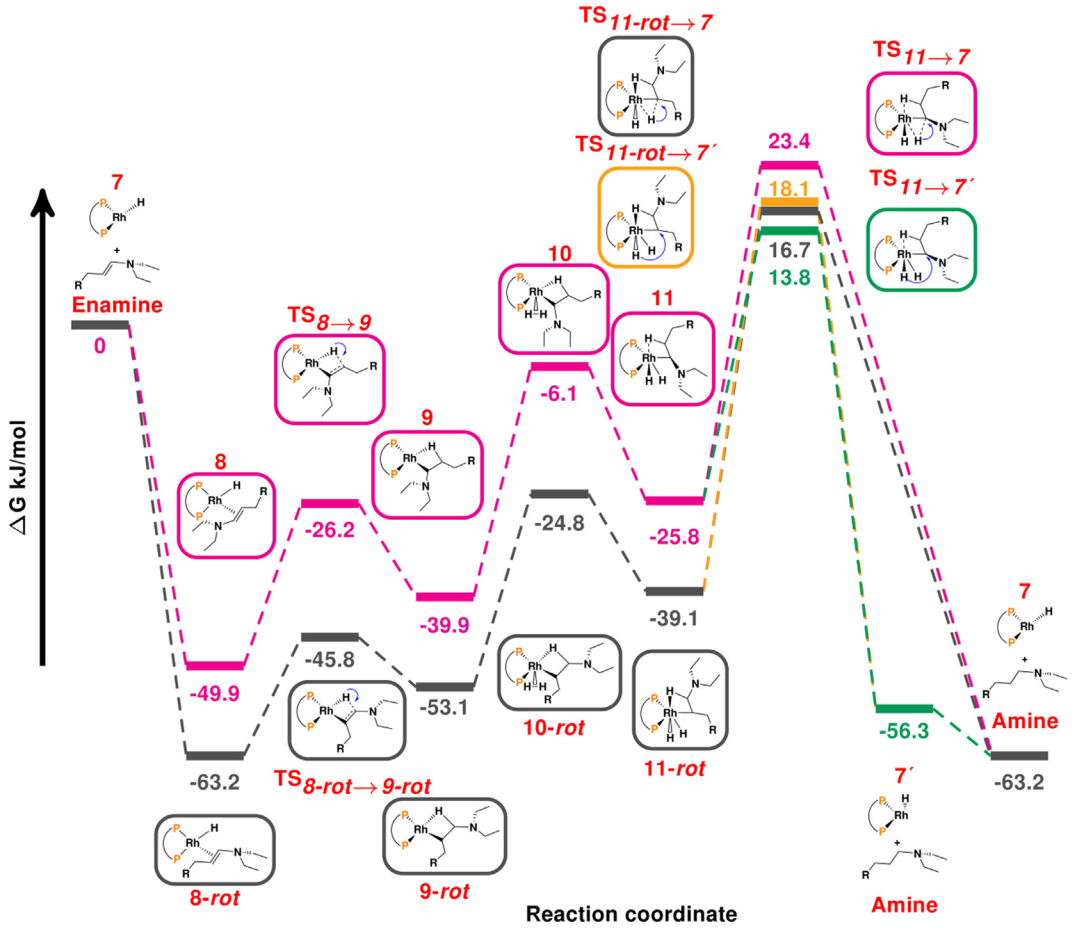

Fig. 8. Gibbs free energy potential energy landscape for (SulfoXantPhos)RhH catalyzed reduction of (E)-*N*,*N*-diethylundec-1-en-1-amine in kJ/mol .

($\Delta G^{\ddagger}_{TS11-rot\rightarrow 7}$ = 55.9, 56.7, and 55.6 in methanol dodecane 0:100, 50:50 and 99:01 solvent mixtures). However, there is a minor increase by 0.5, 3 and 4 kJ/mol for **TS 11-rot** → **7**′ in dodecane methanol 100:0, 50:50 and 1:99 solvent mixtures, respectively.

From Fig. 8 it becomes clear that the formation of ***8-rot*** may thermodynamically be favored, but the subsequent steps following **8** are show lower transition state barriers for the migration of the hydride to C_α ($\Delta G^{\ddagger}$ = 49.2 and 39.5 kJ/mol) are kinetically preferred over C_β ($\Delta G^{\ddagger}$ = 55.8 and 57.2 kJ/mol) in absence of solvents.

The final amine product release is exothermic by −24.1 and −37.4 kJ/mol in the absence of solvent. In solution, the Gibbs free energy for the product dissociation following **TS 11** → **12** further decreases by 12, 14.6, and 11.8 kJ/mol. Similarly, following **TS 11-*rot*** → **12-*rot*** it decreases by 15, 17, and 16.2 kJ/mol in pure dodecane, methanol:dodecane 50:50 and 99:01 solvent mixtures.

The overall activation energy barriers for catalytic reduction of enamine are dependent on the exact reaction mechanism (in the range between 14 and 23 kJ/mol) but all are in good agreement with the experimental activation energy of 19.7 kJ/mol [21].

3.4. Overall control of the reductive amination process by choice of solvent

Fig. 9 shows the global influence of solvent on all individual steps, intermediates, and transition states for the full reductive amination reaction of 1-undecanal and diethylamine by (SulfoXantPhos)RhH. For comparison, we show the results in the absence of explicit and implicit solvation and the optimal reaction path with explicit methanol coordination during the amination part and implicit solvation at the experimental methanol:dodecane 99:1 composition.

The Gibbs free energy profile for the reductive amination via the ***8-rot*** route is given in the SI plus further Gibbs free energies profiles at different solvent compositions.

The Gibbs free energy for substrates association (**2₃**) is higher by 7 kJ/mol in solution but only due to implicit solvation screening charge interactions (see above). The activation energy barrier for nucleophilic addition ($\boldsymbol{TS_{2_3\rightarrow 3_3}}$) decreases by 122 kJ/mol in solution as the solvent molecules actively participate in proton transfer and stabilize the transition via explicit hydrogen bonds. Implicit solvation does not affect the Gibbs free energy of hemiaminal formation ($\Delta G_{2_3\rightarrow 3_3}$ = -4 kJ/mol). With direct methanol coordination, the condensation step occurs in a stepwise rather than a concerted manner. The activation energy barrier for this path is more than 130 kJ/mol lower than concerted one.

The Gibbs free energy of enamine formation is 56 kJ/mol more negative in solution compared to the gas phase, making it the most solvent-sensitive reaction step and thus shifting the thermodynamic equilibrium towards the enamine side.

In the hydrogenation part, the Gibbs free energy for enamine binding (**5₃** → **8**) to the catalyst is most favorable in absence of implicit solvent modelling (by 20 kJ/mol) due to desolvation penalties of catalyst and substrate. The first hydride migratory insertion ($\boldsymbol{TS_{8-9}}$) is almost independent of the consideration of solvation (an effect of 2 kJ/mol). Also the Gibbs free energy required to generate the alkylamine complex **9** only increases by 5 kJ/mol in methanol:-dodecane. Implicit solvation facilitates H_2 coordination to the alkylamine by 4 kJ/mol. The formation of the octahedral rhodium-alkylamine-dihydride complex **11** also benefits from an implicit

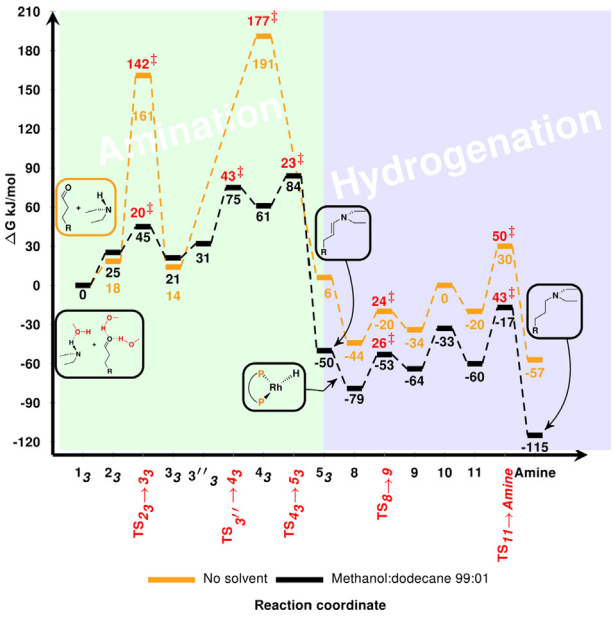

Fig. 9. Solvent effects on the Gibbs free energy profile of the reductive amination of 1-undecanal and diethylamine in the presence of (SulfoXantPhos)RhH in methanol dodecane 99:01 w/w solution. All energies are given in kJ/mol.

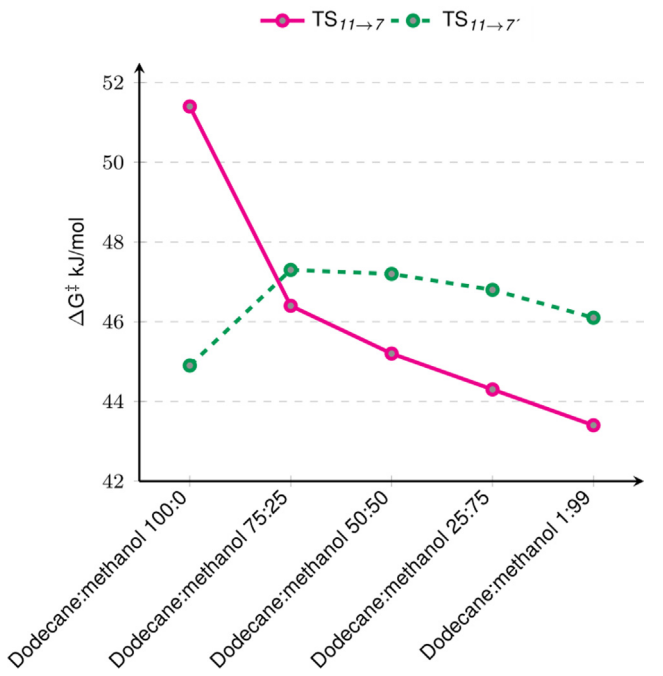

Fig. 10. Solvent control of the transition state barrier of the rate-determining step TS_{11} (reductive elimination of amine) in kJ/mol.

solvation as the Gibbs required for H_2 oxidative addition reduces from 14 to 4 kJ/mol.

Since the final reductive elimination (see Fig. 9) is the rate-determining step for the reaction, we explicitly performed a solvent screening of the height of the activation energy barrier of this transition state for both equatorial and axial hydride migration to C_α of alkylamine. By varying the composition of polar and non-polar components, an optimum solvent composition for reductive amination can be suggested (Fig. 10). Since hydrogenation is only kinetically feasible when the hydride migrates to the C_α of alkylamine (see above), we only consider the product formation via **TS 11 → 7** and **TS 11 → 7′**.

The solvent stabilization of the transition state geometry is significant when the axial hydride (**TS 11 → 7**) migrates to the alkylamine forming the final amine product. Upon increasing the methanol content from 0 to 25 wt%, the barrier is reduced by 5 kJ/mol and by a further 1, 2, and 3 kJ/mol when increasing the polar solvent content. Thus, the activation energy barrier for the rate-limiting step is reduced by 8 kJ/mol in dodecane:methanol 1:99 mixture compared to pure dodecane. Such a kinetic control in polar media was also reported in a recent solvent selection study for XantPhos catalyzed reductive amination [38].

In contrast, with the increase of methanol content from 0 to 25 wt % in the reaction mixture, the activation energy barrier for equatorial hydride migration at first increases by 2.3 kJ/mol, which later slightly decreases when the methanol content is further increased. In the absence of solvent, the equatorial hydride migratory insertion is kinetically favored. However, in solution, the axial hydride migration pathway appears feasible with simultaneous catalyst regeneration as the activation energy barrier is slightly lower. In principle, more polar solvents such as DMF and water might even further lower this activation energy. However, DMF considerably reduces the concentration of active catalyst in the reaction mixture (see above), and water as a side product of amination would shift the chemical equilibrium towards the substrate side.

For the entire reductive amination Gibbs free energy in solution (Fig. 9), enamine formation and amine product elimination steps display transition state barriers of equal magnitude (45 vs. 43 kJ/mol). This is in agreement with a recent experimental kinetic parameter estimation study [21]. This information can only be rationalized by quantum chemical calculations when solvent and solvation effects are fully considered. Gas-phase calculations or only implicit solvent modeling cannot reproduce this experimental observation.

4. Summary and conclusions

In this study, the complete reaction mechanism of the reductive amination process was resolved for the first time. Previous investigations were focusing on either the amination or the reduction part only. When modeling the undecanal and diethylamine reaction with (SulfoXantPhos)RhH and molecular hydrogen as a reducing agent in full detail, a particular emphasis was on the multitude of roles of solvent in this process. The possibilities of solute–solvent interactions and control of thermodynamics and kinetics by solvent were resolved for each elementary step.

In the amination part, explicit solvent coordination significantly promotes the thermodynamics of the association complex formation by increasing the electrophilicity of the carbonyl carbon atom. The explicitly coordinated solvent molecules reduce the activation energy barriers via direct participation in the amination reaction. An optimum of three explicit methanol molecules can directly interact with substrates, fully completing the first solvation shell. The solvent molecules actively assist the intramolecular proton transfer and the condensation reaction and make the latter stepwise rather than concerted.

In the transition metal-catalyzed reduction step, solvent coordination to the catalyst is required to be weak in order to enable substrate access to the rhodium catalyst atom. The SulfoXantPhos ligand is controlling the catalyst's selectivity by its steric demand and enforces particular substrate-ligand interactions. The final reductive elimination step of the amine product is rate-limiting and controlled by solvent-product and ligand-substrate interactions. The hydride approaching C_α instead of C_β of the alkylamine intermediate is kinetically favored, and the activation energy of this rate-limiting step is significantly reduced in polar media. With

reductive elimination as the rate-determining, the control of the kinetic of this elementary step can drive the yield of the entire process.

Methanol as a polar and hydrogen bonding solvent significantly influences the thermodynamics and kinetics of the overall reductive amination process and drives the reaction via a smooth and shallow potential energy surface, thus ensuring high yields and productivity. In addition, methanol as a green solvent will reduce the environmental impact of the reaction, thus promoting the conceptualization and design of modern sustainable processes.

The reductive amination reaction serves as an example reaction here to demonstrate the multiple roles that solvents can play in a reaction mechanism. Substrate-solvent and catalyst-solvent interactions must be energetically balanced to enable a fast turnover and avoid the formation of sideproducts.

CRediT authorship contribution statement

Froze Jameel: Methodology, Investigation, Formal analysis, Visualization, Writing – original draft, Writing – review & editing. **Matthias Stein:** Conceptualization, Funding acquisition, Resources, Formal analysis, Validation, Supervision, Writing – review & editing.

Declaration of Competing Interest

The authors declare that they have no known competing financial interests or personal relationships that could have appeared to influence the work reported in this paper.

Acknowledgements

Gefördert durch die Deutsche Forschungsgemeinschaft (DFG) - TRR 63 “Integrierte chemische Prozesse in flüssigen Mehrphasensystemen” (Teilprojekt A4) - 56091768.

Funded by the Deutsche Forschungsgemeinschaft (DFG, German Research Foundation) - TRR 63 “Integrated Chemical Processes in Liquid Multiphase Systems” (subproject A4) – 56091768.

We thank the Max Planck Society for the Advancement of Science for financial support.

Appendix A. Supplementary material

Supplementary data to this article can be found online at https://doi.org/10.1016/j.jcat.2021.11.010.

References

[1] U. Biermann, U. Bornscheuer, M.A.R. Meier, J.O. Metzger, H.J. Schäfer, Angew. Chem. Int. Ed. 50 (2011) 3854–3871.
[2] United Nations, General Assembly, Transforming our world: the 2030 Agenda for Sustainable Development, Transforming our world: the 2030 Agenda for Sustainable Development (2015). https://sdgs.un.org/2030agenda.
[3] K.S. Hayes, Appl. Catal. A 221 (2001) 187–195.
[4] K.U. Künnemann, J. Bianga, R. Scheel, T. Seidensticker, J.M. Dreimann, D. Vogt, Org. Process Res. Dev. 24 (2020) 41–49.
[5] G. Hahn, P. Kunnas, N. de Jonge, R. Kempe, Nat. Catal. 2 (2019) 71–77.
[6] E. Boz, N.Ş. Tüzün, M. Stein, RSC Adv. 8 (2018) 36662–36674.
[7] Y.-Q. Ding, Y.-Z. Cui, T.-D. Li, J. Phys. Chem. A 119 (2015) 4252–4260.
[8] D. Crozet, C.E. Kefalidis, M. Urrutigoity, L. Maron, P. Kalck, ACS Catal. 4 (2014) 435–447.
[9] T. Irrgang, R. Kempe, Chem. Rev. 120 (2020) 9583–9674.
[10] T. Gross, A.M. Seayad, M. Ahmad, M. Beller, Org. Lett. 4 (2002) 2055–2058.
[11] S. Ogo, K. Uehara, T. Abura, S. Fukuzumi, J. Am. Chem. Soc. 126 (2004) 3020–3021.
[12] J. Gallardo-Donaire, M. Ernst, O. Trapp, T. Schaub, Adv. Synth. Catal. 358 (2016) 358–363.
[13] J. Bódis, L. Lefferts, T.E. Müller, R. Pestman, J.A. Lercher, Catal. Lett. 104 (2005) 23–28.
[14] B. Dong, X. Guo, B. Zhang, X. Chen, J. Guan, Y. Qi, S. Han, X. Mu, Catalysts 5 (2015) 2258–2270.
[15] Y. Nakamura, K. Kon, A.S. Touchy, K.-I. Shimizu, W. Ueda, ChemCatChem 7 (2015) 921–924.
[16] M. Chatterjee, T. Ishizaka, H. Kawanami, Green Chem. 18 (2016) 487–496.
[17] S. Nishimura, K. Mizuhori, K. Ebitani, Res. Chem. Intermed. 42 (2016) 19–30.
[18] G. Liang, A. Wang, L. Li, G. Xu, N. Yan, T. Zhang, Angew. Chem. Int. Ed. 56 (2017) 3050–3054.
[19] T. Komanoya, T. Kinemura, Y. Kita, K. Kamata, M. Hara, J. Am. Chem. Soc. 139 (2017) 11493–11499.
[20] E.J. Schwoegler, H. Adkins, J. Am. Chem. Soc. 61 (1939) 3499–3502.
[21] S. Kirschtowski, F. Jameel, M. Stein, A. Seidel-Morgenstern, C. Hamel, Chem. Eng. Sci. 230 (2021) 116187.
[22] T. Riermeier, K.-J. Haack, U. Dingerdissen, A. Börner, V. Tararov, R. Kadyrov, Patent WO 01/05741 (2001), to Aventis Research & Technologies GmbH & Co KG.
[23] S.A. May, M.D. Johnson, J.Y. Buser, A.N. Campbell, S.A. Frank, B.D. Haeberle, P.C. Hoffman, G.R. Lambertus, A.D. McFarland, E.D. Moher, Org. Process Res. Dev. 20 (2016) 1870–1898.
[24] M.D. Johnson, S.A. May, B. Haeberle, G.R. Lambertus, S.R. Pulley, J.R. Stout, Org. Process Res. Dev. 20 (2016) 1305–1320.
[25] K. Murugesan, Z. Wei, V.G. Chandrashekhar, H. Neumann, A. Spannenberg, H. Jiao, M. Beller, R.V. Jagadeesh, Nat. Commun. 10 (2019) 5443.
[26] J. Gallardo-Donaire, M. Hermsen, J. Wysocki, M. Ernst, F. Rominger, O. Trapp, A. S.K. Hashmi, A. Schäfer, P. Comba, T. Schaub, J. Am. Chem. Soc. 140 (2018) 355–361.
[27] T. Senthamarai, K. Murugesan, J. Schneidewind, N.V. Kalevaru, W. Baumann, H. Neumann, P.C. Kamer, M. Beller, R.V. Jagadeesh, Nat. Commun. 9 (2018) 1–12.
[28] X. Tan, S. Gao, W. Zeng, S. Xin, Q. Yin, X. Zhang, J. Am. Chem. Soc. 140 (2018) 2024–2027.
[29] L. Mark, J. Bakos, J. Organomet. Chem. 81 (1974) 411–414.
[30] S. Kirschtowski, C. Kadar, A. Seidel-Morgenstern, C. Hamel, Chem. Ing. Tech. 92 (2020) 582–588.
[31] P. Kalck, M. Urrutigoïty, Chem. Rev. 118 (2018) 3833–3861.
[32] J. Bianga, N. Kopplin, J. Hülsmann, D. Vogt, T. Seidensticker, Adv. Synth. Catal. 362 (2020) 4415–4424.
[33] M. Ahmed, A.M. Seayad, R. Jackstell, M. Beller, J. Am. Chem. Soc. 125 (2003) 10311–10318.
[34] M. Schreuder Goedheijt, P.C.J. Kamer, P.W.N.M. van Leeuwen, J. Mol. Catal. A: Chem. 134 (1998) 243–249.
[35] M.P. Patil, R.B. Sunoj, J. Org. Chem. 72 (2007) 8202–8215.
[36] J.A. Fuentes, P. Wawrzyniak, G.J. Roff, M. Bühl, M.L. Clarke, Catal. Sci. Technol. 1 (2011) 431.
[37] K. Murugesan, Z. Wei, V.G. Chandrashekhar, H. Jiao, M. Beller, R.V. Jagadeesh, Chem. Sci. 11 (2020) 4332–4339.
[38] F. Huxoll, F. Jameel, J. Bianga, T. Seidensticker, M. Stein, G. Sadowski, D. Vogt, ACS Catal. 11 (2021) 590–594.
[39] S. Song, Y. Wang, N. Yan, Mol. Catal. 454 (2018) 87–93.
[40] S.S. Azimova, A.I. Glushenkova, V.I. Vinogradova, Lipids, Lipophilic Components and Essential Oils from Plant Sources, Springer, London, 2012.
[41] Turbomole v. 7.4 2019, A development of University of Karlsruhe and Forschungszentrum Karlsruhe GmbH, 1989–2007, since 2007 available from TURBOMOLE GmbH (www.turbomole.com).
[42] C. Adamo, V. Barone, J. Chem. Phys. 110 (1999) 6158–6170.
[43] M. Ernzerhof, G.E. Scuseria, J. Chem. Phys. 110 (1999) 5029–5036.
[44] S. Grimme, J. Antony, S. Ehrlich, H. Krieg, J. Chem. Phys. 132 (2010), 154104.
[45] S. Grimme, S. Ehrlich, L. Goerigk, J. Comput. Chem. 32 (2011) 1456–1465.
[46] A. Schäfer, C. Huber, R. Ahlrichs, J. Chem. Phys. 100 (1994) 5829–5835.
[47] S. Dohm, A. Hansen, M. Steinmetz, S. Grimme, M.P. Checinski, J. Chem. Theory Comput. 14 (2018) 2596–2608.
[48] J.J.P. Stewart, L.P. Davis, L.W. Burggraf, J. Comput. Chem. 8 (1987) 1117–1123.
[49] K. Fukui, Acc. Chem. Res. 14 (1981) 363–368.
[50] A. Hellweg, J. Comput. Chem. 34 (2013) 1835–1841.
[51] J.R. Pliego, J.M. Riveros, J. Phys. Chem. A 105 (2001) 7241–7247.
[52] A. Klamt, G. Schüürmann, J. Chem. Soc. Perkin Trans. 2 (1993) 799–805.
[53] A. Klamt, V. Jonas, T. Bürger, J.C. Lohrenz, J. Phys. Chem. A 102 (1998) 5074–5085.
[54] A. Hellweg, F. Eckert, AIChE J. 63 (2017) 3944–3954.
[55] J.A. Fuentes, P. Wawrzyniak, G.J. Roff, M. Bühl, M.L. Clarke, Catal. Sci. Technol. 1 (2011) 431–436.
[56] J. Hine, F.A. Via, J.K. Gotkis, J.C. Craig, J. Am. Chem. Soc. 92 (1970) 5186–5193.
[57] G. Lu, R.Y. Liu, Y. Yang, C. Fang, D.S. Lambrecht, S.L. Buchwald, P. Liu, J. Am. Chem. Soc. 139 (2017) 16548–16555.